Journal of Engineering Science and Technology
Vol. 15, No. 2 (2020) 1296 - 1318

DEVELOPMENT OF NOVEL DESIGN AND FRAME STRUCTURAL ASSESSMENT ON MITUTOYO'S AUTO CHECKING HARDNESS MACHINE USING REVERSE ENGINEERING APPROACH: SERIES HR-522 HARDNESS TESTER

BERNANDUS PLASENTA PREVIO CAESAR,
HASHFI HAZIMI, HERU SUKANTO, ADITYA RIO PRABOWO*

Department of Mechanical Engineering, Universitas Sebelas Maret,
Jl. Ir. Sutami 36A, Surakarta, Central Java 57126, Indonesia
*Corresponding Author: aditya@ft.uns.ac.id

Abstract

The hardness-checking machine is one of the vital tools in mechanical and manufacturing industries, especially in terms of the quality control process. This tool is generally used to measure and standardise the hardness quality of fundamental material, which is subjected for further handling and treatment. Concern to the operability process of manual hardness tester is found in Department of Quality Control in Akebono Brake Astra Indonesia where the manual tester requires more than one machine to complete a testing task which leads to a condition that longer testing time occurs if no machine is added, and wider space is demanded for more tester if new manual machines arrives. Considering those issues, this paper studies a reverse engineering process of manual hardness tester to design a novel auto-checking hardness machine, to reduce other manual devices into one auto-machine using 3D mechanical design. The idea of auto-checking hardness machine is based on a three axes mechanism using Festo linear actuator with a servo motor. The capacity of this machine is six or more of brake pads depending on their type or dimension. The frame of auto-checking hardness machine is assessed by applying load variations, which the results indicate that the lower frame load produces significant structural response than the mounting point on the lower frame. Calculation using finite element analysis and reverse engineering analysis based on benchmarking from a similar simulation of the novel design. It concludes that the structure of the assembled Festo linear actuator is durable and has the innovation of auto checking hardness machine has time processing faster than manual machines.

Keywords: Auto checking hardness, Component displacement, Critical stress, Finite Element Method (FEM), Operating time prediction, Reverse engineering.

1. Introduction

Material testing and analysis [1-7] are critical processes in the design of any technical instrument and machine, which hardness characteristic is one of the essential criteria in engineering practice. Hardness is the properties of materials to resist deformation and destruction [8]. It also defined as the ability of the material to resist elastic deformation, plastic deformation, press-in or scratch. Hardness testing with a manual instrument applies a non-destructive test that does not inflict damage to the material. The development of modern industry makes hardness tester sector drives their innovation and technology to fulfil society demands. Most industries deploy manual hardness tester [9-11] since the manual version is cheaper than the new automatic hardness tester. Nevertheless, it makes the application of manual hardness tester need more devices.

The manual hardness tester has a single capacity, and it pushes the industry to provide more devices since simultaneous hardness checking is more efficient. The product for hardness checking is approximately 10% of the massive production of a day for a sample product, and time cycle of more manual hardness tester is increasing. Therefore, it takes more time to finish checking, and so as the workspace of the more manual hardness tester. Manual hardness tester has to be operated consistently, for example in Akebono Brake Astra Indonesia, which the industry uses 6 Mitutoyo hardness tester and has two operators for a day, and in fact, this condition is time consuming and man-power exhausting. Considering the actual case, demand for a comprehensive hardness instrument to provide the best performance is the research opportunity addressed for production and industry manufacture development.

This paper provides reverse engineering study of a manual hardness tester to be re-designed as an auto-checking hardness machine. The auto checking hardness machine adopts a conventional tester with the modification of the lifting mechanism. The auto checking machine applies the three-axes-moving mechanism with the Festo actuator and motor. The novel design is projected to be capable of replacing the manual tester as providing auto-checking hardness machine with more capacity and less processing time.

2. Literature Review

2.1. Pioneer research and patent

The core of this design follows of CNC with 3-axes mechanism. It is similar to design of a micro machine tool with double-toggle mechanism by Wang [12] and static structural analysis of great five-axis turning-milling complex CNC machine by Hong [13]. The concept is also found in Indonesian Patent Rights which is translated to a design of automatic greenhouse using CNC machine with arm integrated of BLYNK software on android software for farming productivity [14] and utilization of electronic waste to be CNC machine 3-axes prototype as an educational media [15]. In these previous works, the application of servo motors is deployed as a source of moving instrument, while linear drive and linear guide as a mover in automatic system of 3-axes mechanism.

2.2. A variety of hardness test

Scratch hardness [16] is the measurement of material ability subjected to fracture or permanent plastic deformation by friction from sharp objects. The principle is

that an object made of a harder material will scratch an object composed of a softer material. The value of the scratch hardness test is the force needed to cut through the film to the substrate [8].

Indentation hardness is the measurement of resistance to material deformation due to a constant compression load from an indenter. The principle of the indentation hardness method is determined based on static load from indenter into a material sample. There are three standard indentation hardness scales, i.e. Rockwell ASTM-E18, Vickers ASTM-E384, and Brinell ASTM-E10 [17-19]. These test methods of ASTM-E18 cover the determination of Rockwell superficial hardness of metallic by the Rockwell indentation hardness principle. Rockwell hardness test is determined by the depth of penetration of an indenter under a significant load compared to the penetration of a minor load (see Eq. (1)). The result is the dimensionless number noted as HR.

$$HR = E - e \tag{1}$$

The Brinell hardness test is the indentation hardness test of materials loaded constantly in 500 – 3000 kgf with 10 mm diameter steel ball indenter (see Eq. (2)). The principle of the test measures the diameter of penetration by microscope. The Brinell test ASTM-E10 method covers the determination of the Brinell hardness of metallic materials by the Brinell indentation hardness principle [18].

$$BHN = \frac{2P}{\pi D\left(D - \sqrt{D^2 - d^2}\right)} \tag{2}$$

Vickers hardness test is the indentation hardness test of materials to measure the high hardness material loaded by diamond pyramid indenter 1-120 kgf (see Eq. (3)) which will be processed in 10-15 s. The principle of the test is the length of penetration due to indentation [18]. The Vickers ASTM-E384 method covers micro indentation tests made with Knoop and Vickers indenters under test forces in the range from 9.8×10^{-3} to 9.8 N (1 to 1000 kgf) [19, 20].

$$HV = \frac{1.8544P}{d^2} \tag{3}$$

Rebound hardness, also known as dynamic hardness is the measurement of the height of the bounce of a diamond-tipped hammer which is dropped from a fixed height into the material. The device used to measure this measurement is scleroscope [21].

2.3. The fundamental design concept of the reverse engineering

Reverse engineering is the process by which an object is deconstructed to reveal its designs and extract knowledge [22]. However, the reverse engineering process, as such, is not concerned with creating a copy or changing the object in some way. It is an analysis in order to deduce design features from product with novel additional knowledge from original production [22, 23]. Figure 1 shows the reverse engineering design flow for designing Auto Checking Hardness Machine.

Recognition stage of a need to feasibility study is the process of searching for the knowledge and market survey of the reverse engineering product. Design process starts from creative design and detailed design. The creative design means

the sketch design of the product, the preliminary design means the 3D modelling of CAD, detailed design is the result of simulation process. This paper provides the reverse engineering design flow process until detailed design [22]. These concepts will be applied to an actual case in the Quality Control (QC) of Akebono Brake Astra Indonesia, where the worker operates six manual hardness tester (see Fig. 2). As the characteristic of the manual test is single operation, each tester has to be operated separately. Tester using conventional concept also requires more spaces. Based on the concept of reverse engineering, a knowledge to develop a novel design that satisfies the requirements of manual hardness instrument. Therefore, there will be an enhancement of the manual instrument with those studies.

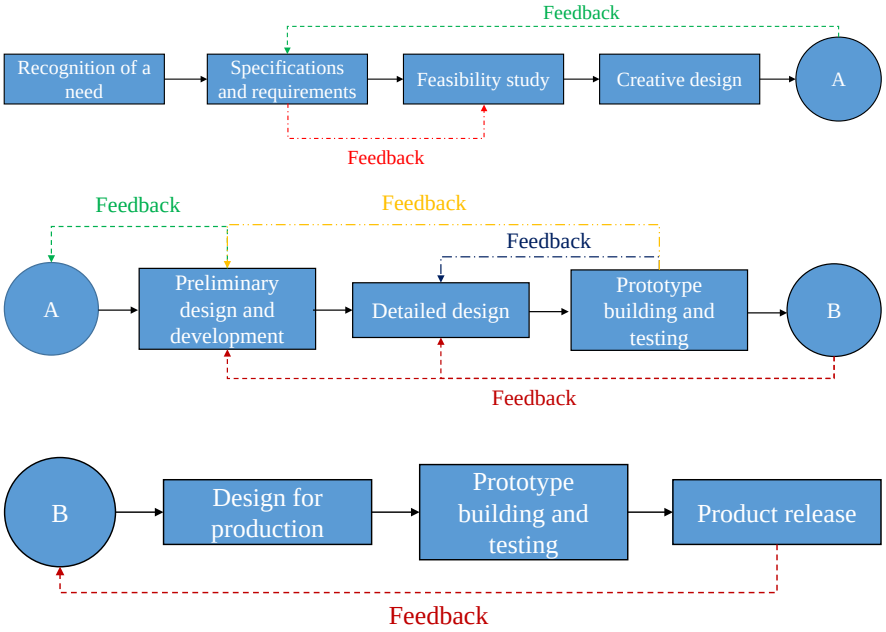

Fig. 1. Design flow of reverse engineering process based on literature [22].

Fig. 2. Actual situation as reference for application of reverse engineering concept in the current study.

The goal of reverse engineering from this case is re-design the manual instrument with some additional for automatic instrument. The 3-axes mechanism (X-Y-Z) using Festo linear actuator and servo motor is added to the manual instrument with alteration the manual system to the automatic system using computer program and PLC (Programmable Logic Controller) program [24, 25]. The capacity of an auto system machine is 6 pieces in a single testing cycle, in which the auto system machine is capable of replacing six manual testers. The cycle time of the auto system will be reduced compared to manual system machine as six pieces of specimen are possibly tested simultaneously. The dimensions of an auto system machine are smaller than six manual hardness machines with reduction in workbench area (170 × 820) mm^2. An operator will replace the specimen on the auto tester, and the tester operates automatically and produces the hardness results.

2.4. Applied engineering terminologies

2.4.1. Active force and related response on the structures

The force on the vertical axis (see Eq. (4)) is the result of mass and acceleration of gravity or the working forces on the vertical axis [26], while the force on the horizontal axis (see Eq. (5)) is the result of mass and acceleration or the working forces on the horizontal axis.

$$\Sigma F = 0, \quad F_y = m \cdot g, \quad F_x = m \cdot a \tag{4}$$

$$\Sigma M = 0, \quad M_x = F \cdot l \tag{5}$$

The moment force of the *x-axis* or *x-point* is the results of force in perpendicular direction and distance of the force and *x-point*.

2.4.2. Stress and strain equation for frame structure analysis

The normal stress (as shown in Eq. (6)) is obtained by dividing the magnitude *P* of the load by the cross-sectional area *A* [26]. The shearing stress as shown in Eq. (7), is a component of stress with a material cross-section [27]. Shear stress arises from the force vector component parallel to the cross-section of the material [26, 27]. Normal strain considering rod length *(L)*, uniform cross-section, and deformation is defined by the normal strain *(ε)* in the rod as the deformation per unit length. Elasticity *E* in Eq. (8) is the ratio of normal stress and occurred strain.

$$\sigma = \frac{P}{A}, \quad \tau = \frac{F}{A} \tag{6}$$

$$\varepsilon = \frac{\delta}{L} \tag{7}$$

$$E = \frac{\sigma}{\varepsilon} \tag{8}$$

2.4.3. Deformation under transverse loading

Y(x) is the vertical deflection of a point on the neutral axis of a beam [27]. Thus, the internal bending moment provides a quantitative indicator of how curvature, d^2y/dx^2, varies along a beam. The product *El* is known as the flexural rigidity of the beam; C_1

and C_2 are two constant of integration that can be determined from the boundary conditions imposed on the beam by its supports. The maximum deflection is obtained by determining the value of x for which the slope is zero and the corresponding value of y. This description is defined as a mathematical formula in Eqs. (9) to (11).

$$\frac{d^2y}{dx^2} = \frac{M_{(x)}}{EI} \tag{9}$$

$$El\frac{dy}{dx} = \int_0^x M_{(x)}dx + C_1 \tag{10}$$

$$El \cdot y = \int_0^x dx \int_0^x M_{(x)}dx + C_1 + C_2 \tag{11}$$

2.4.4. Deformation under transverse loading

The term *beam* has a very specific meaning in engineering mechanics as the component that is designed to support form the loads like transverse loads, applied force or pressure and distribution force. The beam support may vary in form of roller support, pin support and cantilever mode support [27, 28]. For every external load applied to the beam, the beam generates internal forces, i.e. normal forces, shear forces and moment. For Timoshenko beam theory, the model takes into account shear deformation and rotational bending effects, making it suitable for describing the behaviour of thick beams subject to high-frequency excitation when the wavelength approaches the thickness of the beam. Figure 3 shows the beam with type of supports and type of forces.

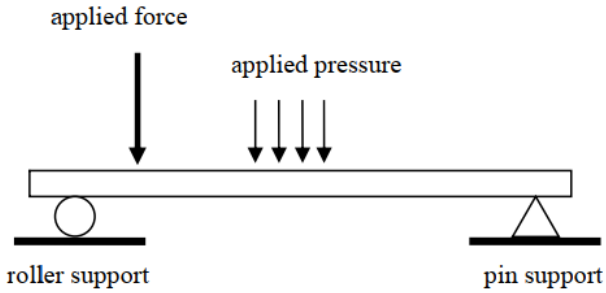

Fig. 3. Supported beam loaded by a force and a distribution pressure.

2.4.5. Static analysis in FEM

The finite element method (FEM) is the most widely method for solving problems of engineering models [29]. To solve a problem, the FEM subdivides a large part into smaller which is implemented by the construction of a mesh of the object. For static calculation which are related with beam theory is the application of state of stress which subdivides the part of beam theory to calculate the stress and strain of the beam [27].

The main goal of static analysis is to check a structure used in machine-building or construction for strength [29]. As a result of solving the problem of modelling, the stress state of the structure and numerous results are available, e.g.: fields of displacements of the structure in nodes of finite-element mesh; fields of strains normal strains, shear

strains, equivalent strains; fields of components of the stresses – normal stresses, shear stresses, equivalent stress (Von Mises Stress); energy of deformation; reaction forces; field of distribution of safety factors by principal stress, safety factor by normal stress, safety factor by equivalent stress. This information is usually sufficient to predict the behaviour of structures and make a decision how to optimize the geometric shape of the product [27, 29]. Figure 4 shows the state of stress, the subdivides part of some force given product. There are normal stress caused by lateral forces and bending moment and shearing stress caused by shear forces and torsional forces.

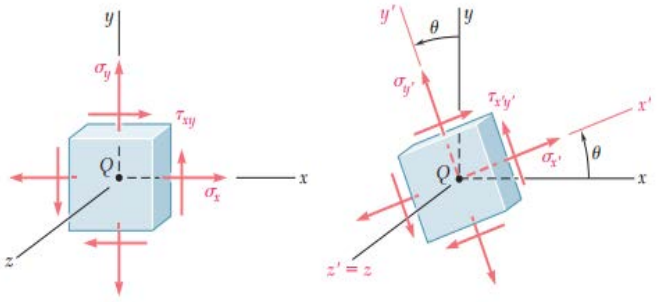

Fig. 4. Schematic illustration of working stress state in a medium.

3. Novel Design

3.1. The proposed design parts

3.1.1. Linear drive

The linear drive is an axis moving mechanism by belt, ball screw, spindle axes, cantilever axes, and combined devices. Generally, it has a horizontal or vertical moving mechanism. The difference of the linear type is the location of mounting system, dimension, function and intrinsic properties. Auto-checking hardness machine uses Festo mini slides EGSC – BS (ball screw) series and Festo spindle axes ELGC – BS (ball screw) – KF (recirculating ball bearing guide) series.

3.1.2. Parallel kit

The parallel kit is a gearbox that connecting servo motor and actuator or linear drive in parallel position. The advantage of using a parallel kit are space effectiveness, easy installation and easy maintenance.

3.1.3. Servo motor

Servo motor is a DC motor with a closed-loop mechanism system that allows control precisely of angular or linear position, velocity, and acceleration. The input to its control is a signal representing the position commanded for the output shaft.

3.1.2. Parallel kit

The parallel kit is a gearbox that connecting servo motor and actuator or linear drive in parallel position. The advantage of using a parallel kit are space effectiveness, easy installation and easy maintenance.

3.1.3. Servo motor

Servo motor is a DC motor with a closed-loop mechanism system that allows control precisely of angular or linear position, velocity, and acceleration. The input to its control is a signal representing the position commanded for the output shaft.

3.1.4. Linear guide

The linear guide is designed to provide free motion in one direction. The linear guide is non-motorized linear slides that provide low-friction linear movement for powered linear drive equipment [24]. The linear guide is based on roller bearing to provide more massive load capabilities and better movement control [25].

3.1.5. Safety sensor

The safety sensor is a sensor to keep the safety of particular machines or tools. A safety sensor consists of a pair of interconnected transmitters and receivers. The principle of safety sensor is to detect the other object, which blocks sensor from the transmitter to the receiver.

3.2. Component parameters detail

3.2.1. Configuration details

Configuration table of linear drive given from Festo and Misumi data specification, which is summarized in Tables 1 and 2. The positions of *x*-, *y*-, and *z*-axes on ELGC – BS - KF Festo linear drive series, EGSC – BS Festo linear drive series, and Misumi linear guides are described in Figs. 5(a) and (b). The parameters presented in Table 1describes configurations of ELGC – BS – KF and EGSC – BS Festo linear drive series (displayed in Fig. 2). The parameters presented in Table 2 presents configurations of Misumi linear guides as displayed in Fig. 5(c). Fx_{max} of linear drive configurations shows the feed force of linear drive, while other parameters show the maximum force which can be held by the linear drive. The linear guide parameters of *C* (dynamic) show an applied load in a constant direction, which run without experiencing any damages due to rolling fatigue. On the other hand, the linear guide parameters of *Co* (Static) show an applied load on non-moving linear guides. The linear guides parameters of M_A, M_B, M_c shows allowable static moment [25].

Table 1. Maximum parameters on ELGC and EGSC linear drives.

Parameter	ELGC linear drive	EGSC linear drive
	Values (N)	
Fx_{max}	200	250
Fy_{max}	600	4937
Fz_{max}	1800	4937
Mx_{max}	29.1	20
My_{max}	31.8	30
Mz_{max}	31.8	30

Table 2. Maximum parameters on linear guides.

Parameter	Value (N)
C (Dynamic)	5200
Co (Static)	8500
Ma_{max}	48.4
Mb_{max}	48.4
Mc_{max}	86.4

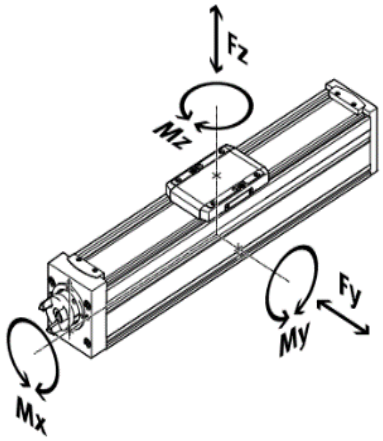

(a) ELGC configuration.

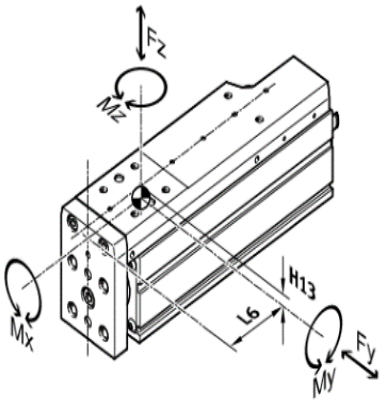

(b) EGSC configuration.

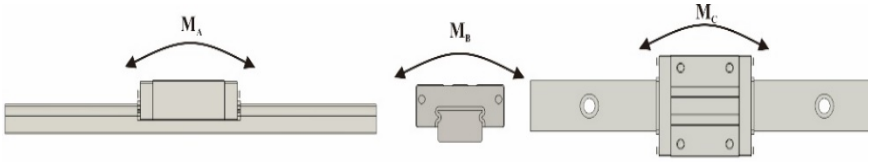

(c) Linear guide configuration.

Fig. 5. Details of the component configuration.

3.2.2. Defined loads

The load is defined as the mass of the component/part presented in Table 3. The mass of six brake pads uses the biggest dimension in the groups of the brake pad type which is generally manufactured for industry used, while all linear drives apply the same type of servo motor, parallel kit, and adapter kit. Misumi linear guides (Y and X masses) cover the linear guide rails, blocks, and base. The linear guide of the Z-axis mass contains Misumi linear bushing MFINS30 series and Misumi shaft. Jig in Table 3 designates the most significant brake pad type. A linear bushing base is a mounting base of linear guide Z-axis. ELFC is Festo linear guide series for guiding Festo linear drive ELGC Y-axis.

Table 3. Defined mass as a working load on the design.

No.	Part	Mass (kg)	No.	Part	Mass (kg)
1	6 Brake pads	2	8	Servo Motor	1.6
2	Base	6	9	Parallel Kit	0.6
3	Jig	2	10	Adapter Kit	0.2
4	EGSC (Z)	3.1	11	Linear Guides (Y)	4.8
5	ELGC (X)	7.9	12	Linear Guides (X)	17.52
6	ELGC (Y)	2.7	13	Linear Guides (Z)	2.66
7	ELFC (Y)	2.2	14	Linear Bushing Base	6.5

3.3. Assembly design and component detail

Each assembly has a linear drive, adapter kit, parallel kit, and servo motor (see Fig. 6). Z-axis assembly applies EGSC Festo linear drive, which is proper to lift the vertical load. X-axis assembly applies ELGC Festo linear drive with 600 mm stroke to fill-up the most significant brake pad width. Y-axis assembly applies ELGC Festo drive and ELFC Festo linear guide with 100 mm stroke to fill-up the most significant brake pad length. Z-axis and X-axis assemblies are connected laterally with an adapter kit. X-axis and y-axis assemblies are connected axially with 2 adapter kits. The adapter kit combines two same-size linear drives (Fig. 7). The auto checking hardness machine is covered by 2 mm metal sheet and a Keyence safety sensor [3]. All three axes of the Festo Linear Drive use the same series Festo Motor-EMMB-AS-60-02-SB, Festo Adapter Kit EHAA-D-L2-60, and Festo Parallel Kit-EAMM-U-T42-60P-87.

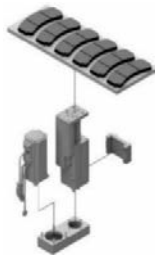

(a) *Z-axis* assembly.

(b) *X-axis* assembly.

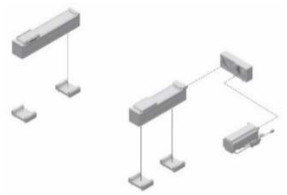

(c) *Y-axis* assembly.

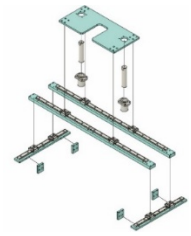

(d) Linear guides assembly.

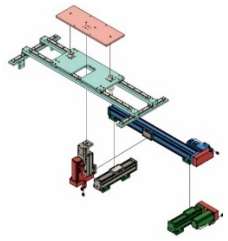

(e) Full component assembly.

Fig. 6. Components for overall design assembly.

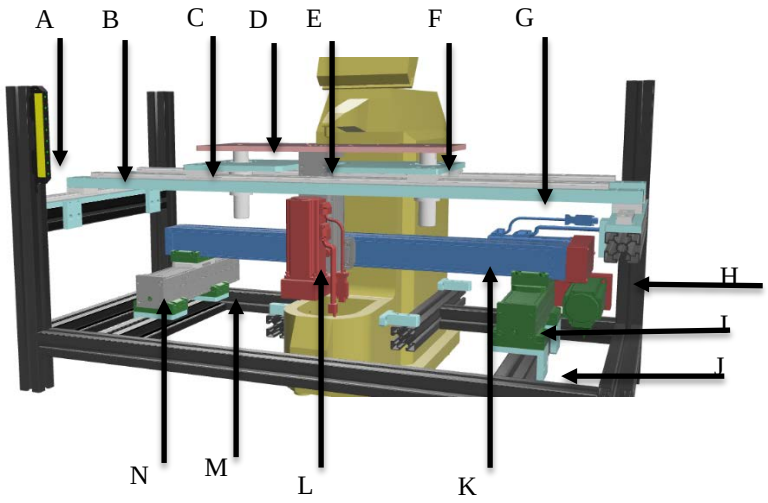

A : Safety Sensor Keyence
B : Misumi LGR SE2B – 400
C : Linear Bushing Base
D : Brake Pad Jig Base
E : Festo EGSC – BS – KF – 60 – 75 – 12P
F : Misumi Linear Bushing MFINS30
G : Linear Guide Base
H : Festo Parallel Kit-EAMM-U-65-T42
I : Festo Linear Drive ELGC-BS-KF-60
J : Mounting to Frame
K : Festo Linear Drive ELGC – BS – KF
L : Festo Motor – EMMB – AS – 60 – 02
M : Festo Adapter Kit EHAA – D – L2
N : Festo Linear Guide ELFC – KF – 60

Fig. 7. Detailed component assembly.

3.4. Time ratio of test processing: manual tester vs. automatic tester

Time ratio in this discussion is defined as comparison between time operations of manual (existing tester in the company) and automatic (re-designed in this study) testers. The manual time processing is based on direct observation in quality control department of Akebono Brake Astra Indonesia (see Fig. 2) while the automatic time processing is based on calculation assumption of 3-axes linear drive moving. The time ratio of processing is calculated by numbers of the checked points on a specimen which is placed on each brake pad. The brake pad hardness checking standard is four-point hardness checking square shaped.

Based on obtained results in Table 4, the automatic processing time is calculated approximately with the difference time 4-6 second for each check point. Reason of time difference between manual and automatic time processing is method of result input. The time used for input manually has a longer time period than the automatic. In the automatic tester, the test result will be inputted automatically to the computer system, while in the manual tester, the result has to be inputted manually by the operator. Results also indicated that larger numbers of checked points, time operation of the automatic tester is found better than time operation of the manual with gap in the largest points 50 s and ratio 1.41.

Table 4. Time ratio of hardness tester performances.

No.	Point numbers (piece)	Manual (s)	Automatic (s)	Ratio
1	1	10	10	1
2	2	18	16	1.125
3	3	26	22	1.18
4	4	32	26	1.23
5	5	40	32	1.25
6	6	48	38	1.26
7	7	56	44	1.272
8	8	60	47	1.276
9	9	64	50	1.28
10	10	70	55	1.29
11	11	78	60	1.3
12	12	84	64	1.31
13	13	90	68	1.323
14	14	97	73	1.328
15	15	104	78	1.33
16	16	110	84	1.34
17	17	118	88	1.341
18	18	126	93	1.35
19	19	134	98	1.36
20	20	142	104	1.36
21	21	150	109	1.37
22	22	158	114	1.385
23	23	164	118	1.389
24	24	170	120	1.41

4. Benchmarking Particulars

The benchmarking uses Shell Eco Marathon urban concept chassis in previous work of [30] for finite element (FE) simulation. This paper [30] provides manual calculation and Autodesk Inventor simulation of the Shell Eco Marathon urban concept chassis, which will be compared by current analysis using its' geometry and setting as verification of current FE methodology. This benchmarking type is considered powerful enough as previously used in finite element analysis even for dynamic structural problems (see references [31-33]). The geometrical model of the Shell Eco Marathon chassis is shown in Fig. 8.

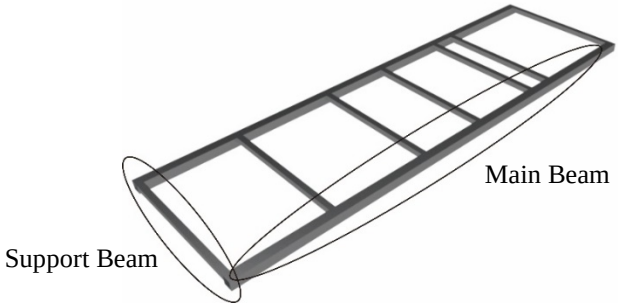

Fig. 8. FE model of the Shell Eco Marathon (SEM) chassis in [29].

The geometry of chassis applies square hollow with 6061 series of aluminium material. Total dimension of the chassis is 2060 x 600 mm with the chassis assembly consists of 2 aluminium 40 × 40 aluminium main beam and 7 aluminium

25 × 25 aluminium support beam [34]. Illustration in Fig. 9 depicts the load distribution on each part of support beam.

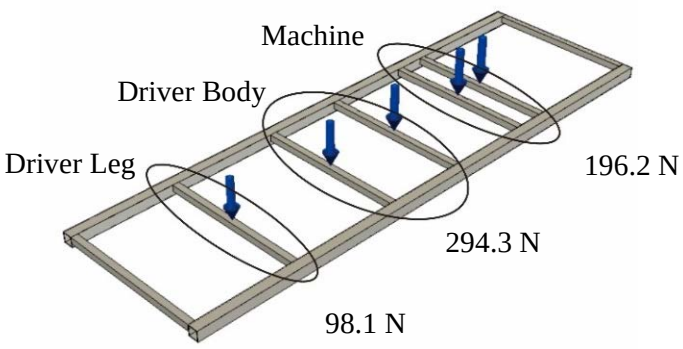

Fig. 9. Loads distribution of Shell Eco Marathon chassis.

Based on the illustration, it also noted that the support beam near the driver leg is loaded by 98.1 N as the assumed mass of driver leg. The driver body is loaded by 294.3 N from the body mass approximately and supported by 2 support beams. Machine's support beam chassis is loaded by 196.2 N from machine mass and supported by 2 support beams [30]. Calculation results of FE simulation is summarized in forms of ratio between manual calculation, simulation of Autodesk Inventor (AI) and simulation of Autodesk Fusion 360 (AF360) which is presented in Tables 5 to 7.

Table 5. Ratio of manual calculation, Autodesk Inventor and Autodesk Fusion 360 for static calculation on machine chassis part.

Structural – design responses	Manual (Previous work in [30])	AI (Previous work in [30])	AF 360 (Current work)	Ratio Between Manual and AF360 (%)	Ratio Between AI and AF360 (%)
Maximum Stress (MPa)	8.48	7.80	6.974	82.24	89.41
Displacement (mm)	0.15	0.08	0.075	50	93.75
Safety Factor	-	15	15	-	100

Table 6. Ratio of manual calculation, Autodesk Inventor and Autodesk Fusion 360 for static calculation on driver body chassis part.

Structural – design responses	Manual (Previous work in [30])	AI (Previous work in [30])	AF 360 (Current work)	Ratio Between Manual and AF360 (%)	Ratio Between AI and AF360 (%)
Maximum Stress (MPa)	12.7	11.71	8.861	69.78	75.67
Displacement (mm)	0.22	0.12	0.095	43.18	79.16
Safety Factor	-	15	15	-	100

Table 7. Ratio of manual calculation, Autodesk Inventor and Autodesk Fusion 360 for static calculation on driver leg chassis part.

Structural – design responses	Manual (Previous work in [30])	AI (Previous work in [30])	AF 360 (Current work)	Ratio Between Manual and AF360 (%)	Ratio Between AI and AF360 (%)
Maximum Stress (MPa)	4.25	3.90	3.487	82.05	89.41
Displacement (mm)	0.07	0.04	0.037	52.86	92.5
Safety Factor	-	15	15	-	100

The result shows that the ratio between previous work and current analysis in terms of FE simulation is satisfying with the lowest ratio is 75.67%. On the other hand, manual calculation in [30] is found quite distinct compared to the numerical simulation. Nevertheless, this tendency is also noted during comparison between manual calculation and simulation in the previous work. Therefore, the current FE methodology is successfully producing good structural estimations.

In order to ensure precise mesh configuration for the extended structural analysis of the developed automatic hardness tester, the second benchmarking is addressed to study the effect of the mesh size in range 5 to 60 to structural response. Location of the tested model is on the driver leg support beam part of the [30]. The mesh sizes which produce stable structural response is projected to be applied in the extended study. Results of the mesh benchmarking is shown in Table 8. Results indicated that the effect of mesh size to structural responses, i.e. maximum stress and displacement is found to less significant in range of mesh size 20-60 mm. Based on this results mesh size of the geometrical model applies this calibrated range.

Table 8. Ratio of mesh size grid length on driver leg chassis part.

Mesh size (mm)	Nodes	Elements	Maximum Stress (MPa)	Displacement (mm)
5	26033	12965	4.780	0.038
10	5896	2920	4.365	0.038
15	2963	1461	3.643	0.038
20	1623	837	3.236	0.037
25	1297	665	3.109	0.037
30	1068	536	3.306	0.037
35	1342	682	3.487	0.037
40	1591	817	3.446	0.037
50	1291	661	3.373	0.037
60	1079	551	3.046	0.037

5. Structural Frame Analysis

5.1. Overall design for FE simulations

After designing a novel design based on the conventional manual tester, analysis of the structural frame on the auto-checking hardness machine with the finite element method using Autodesk Fusion 360 is conducted. The purpose is to ensure the frame structure will transfer loads via nodes, which is to ensure the structure is not affected due to the bending forces [35]. To achieve excellent capability, frame structures are supported by machine with the finite element method using Autodesk Fusion 360 is established.

The purpose of the analysis process is to ensure the frame structure will transfer loads via nodes, which is to ensure the structure is not affected due to the bending forces on side of four legs [34] where loads work on the three-axis mechanism. Figure 10 describes the frame assembly of the auto checking hardness machine. The vertical side frame is made higher to place the safety device. The blue-colour area notes mounting location of the x-y-z linear actuator on the frame. The connection between aluminium profiles uses a special bolt of aluminium profile, and loads of x-y-z linear actuator is carried by steel frame mounting in the bottom side [36].

Loads of the linear guides are held by steel frame mounting at the top side. Figure 11 shows the applied meshing on the frame assembly. The frame meshing has 1745598 nodes and 875321 elements, which also shows the four critical meshing points. The frame meshing has parabolic element order, maximal turn angel on curves 60°, maximal adjacent mesh ratio 1.5, and maximal aspect ratio 10.

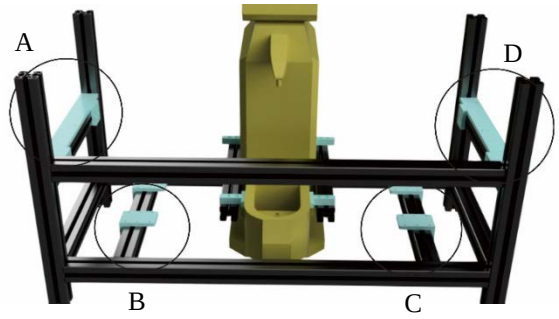

Fig. 10. Frame assembly as analysis subject of the finite element method.

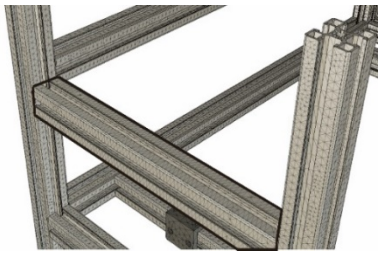

1.745.598 nodes
875.321 elements
(a) Part A.

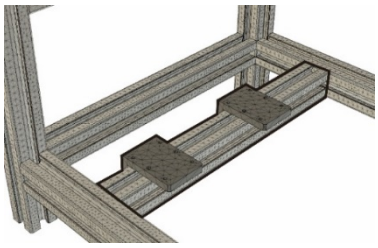

1.745.598 nodes
875.321 elements
(b) Part B.

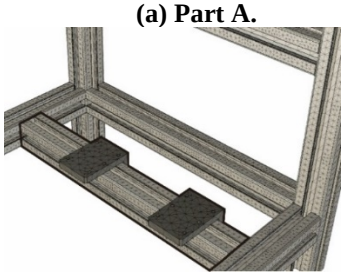

1.745.598 nodes
875.321 elements
(c) Part C.

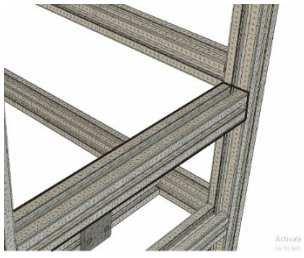

1.745.598 nodes
875.321 elements
(d) Part D.

Fig. 11. Applied meshing on the frame assembly.

5.2. Scenario and boundary condition

The structural analysis uses Autodesk Fusion to conduct the finite element calculation. The idealisation of the structure design and boundary condition is divided into several stages. First, the geometrical model of the Mitutoyo Hardness Tester HR-522 guided by machine blueprint is created. Second, linear drives *x-axis*, *y-axis*, and *z-axis* are inputted on Fusion 360 from Festo website by iges extension to present realistic model. Third, the frame of auto checking hardness machine is combined with the system, which aluminium 45x45 mm with manufacturing standard of the sixth series aluminium (Table 9) is considered as the material of the frame structure. The simulation process applies a static simulation of Autodesk Fusion 360. The materials, loads, and constraints are inputted manually for the preliminary condition for the simulation process.

Table 9. Properties of the sixth series aluminium.

No.	Parameter	Value
1	Density	2.7×10^{-6} kg/mm^3
2	Young's Modulus	6.89×10^4 MPa
3	Poisson's Ratio	0.33
4	Yield Strength	275 MPa
5	Ultimate Tensile Strength	310 MPa

The auto checking hardness machine is supported on the ground by the Misumi level adjuster. There are four level adjusters in 4-arm frame which as presented in Fig. 12, four constraint points are applied on the ground base, and two constraint points on supporting arms of the tester system [37]. Loads are divided into two main types, i.e. centered and distributed types. The loads come from the part that loaded in the topside frame and downside frame. The part which applied in the topside frame is Z-axis linear drive assembly and Z-axis linear guide. The part which applied in the downside frame is XY-axis linear drive assembly and XY-axis linear guide assembly. The centred loads are applied on two arms to the negative direction of the Z-axis with restraint value 26.5 kg. On the other hand, the distributed loads are applied on the top side frame with value 38.87 kg (Fig. 13).

Therefore, the frame of the first scenario is loaded with 259.7 N distributed load divided into two arms on the direction of minus *z-axis*, which each frame load is designated to be 129.85 N [38]. In the second scenario, the frame is loaded with 259.7 N which is distributed to four points of mounting frame on the downside frame. Each mounting frame load has 64.925 N of the centred load. The first and second scenarios have same distributed loads on topside frames while loads of topside frames are 380.89 N divided by two frames, which makes each topside frame endures 190.445 N.

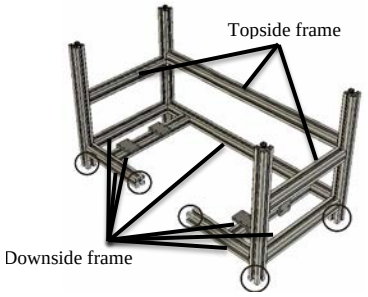

Fig. 12. Locations of the defined constraint system.

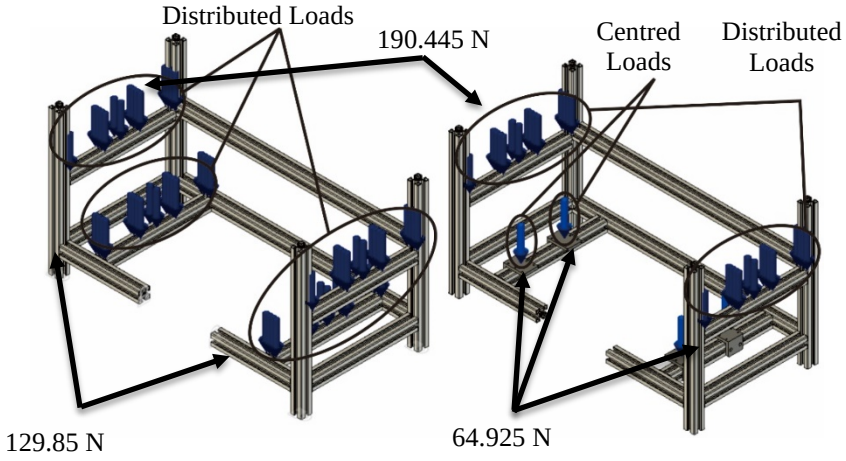

(a) Loads in a frame in scenario 1. **(b) Loads in a frame in scenario 2.**

Fig. 13. Applied load on the structural frame.

6. Results and Discussion

6.1. Scenario and boundary condition

Based on displacement contours (Fig. 14), the frame has a deflection value from range 0 - 1.53 × 10^{-2} mm. The maximal displacement is 1.53 × 10^{-2} mm located in the middle point of the lower frame on the red colour due to the constraint in an endpoint. Figure 14 on part B states the displacement in this area, which is higher than parts A and C due to loads of frame on part B is the most significant. The Stress Von Mises analysis of frame shows that the maximal stress that distributes to the frame has a range from 0-2.77 MPa. The critical stress (Fig. 15) of the frame is in part B aluminium frame. This phenomenon occurs because the distribution of critical stress is equal, the constraint is in the endpoint of each side, and the loads in part B are higher than frame point A. Therefore, simulation analysis on parts A and B indicates that the critical side is on the medial side.

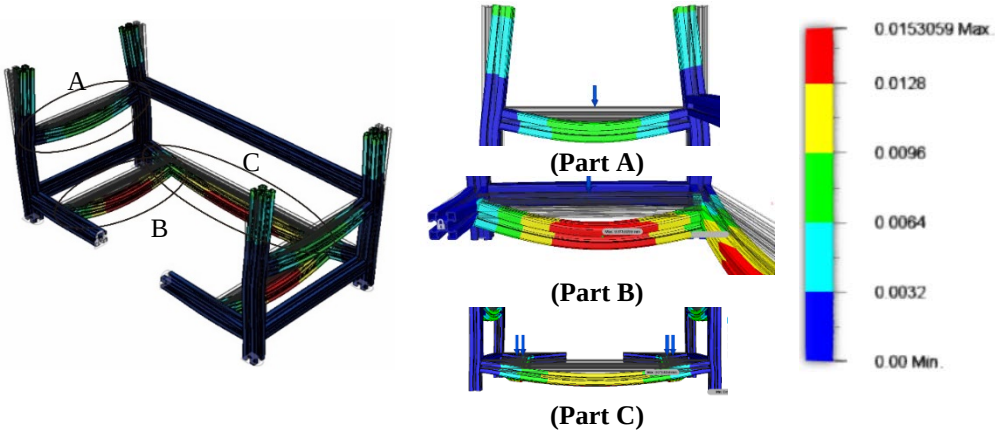

Fig. 14. Frame Simulation: displacement contour of scenario 1.

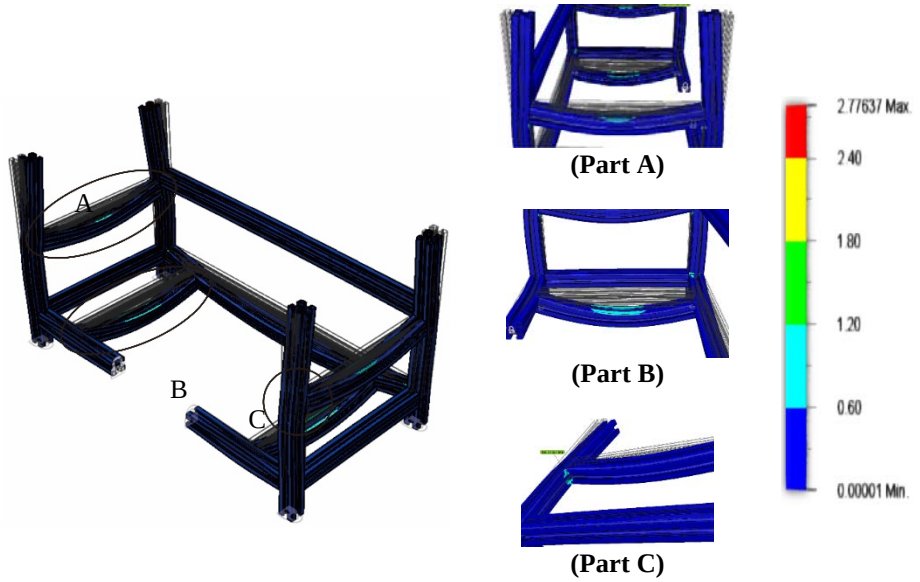

Fig. 15. Frame simulation: stress contour of scenario 1.

6.2. Scenario 2

Based on the results of the second scenario in Figs. 16 and 17, the displacement and Von Mises stress have a smaller value than the first scenario. The maximum displacement is 8.8×10^{-3} mm, 6.5×10^{-3} mm smaller than the first scenario. The topside frame of the second scenario simulation has a critical range that is different from the first scenario due to the lower frame distribution loads of the second scenario is divided by 4 points mounts. Therefore, each point mount has a smaller value than the lower frame distribution load of first scenario.

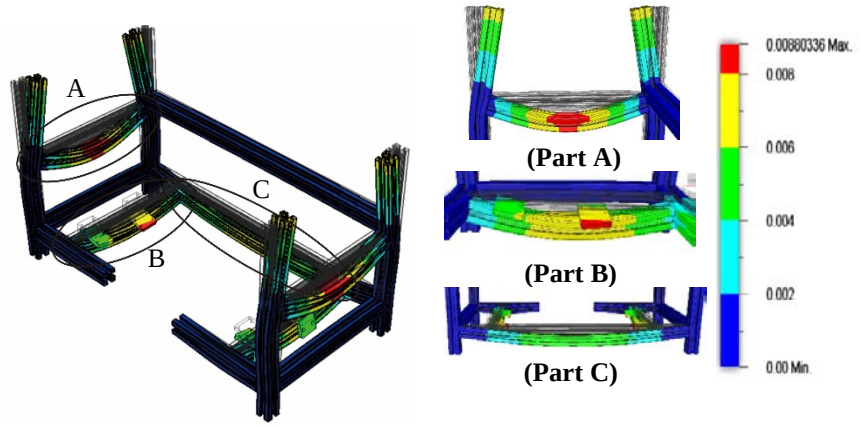

Fig. 16. Frame simulation: displacement contour of scenario 2.

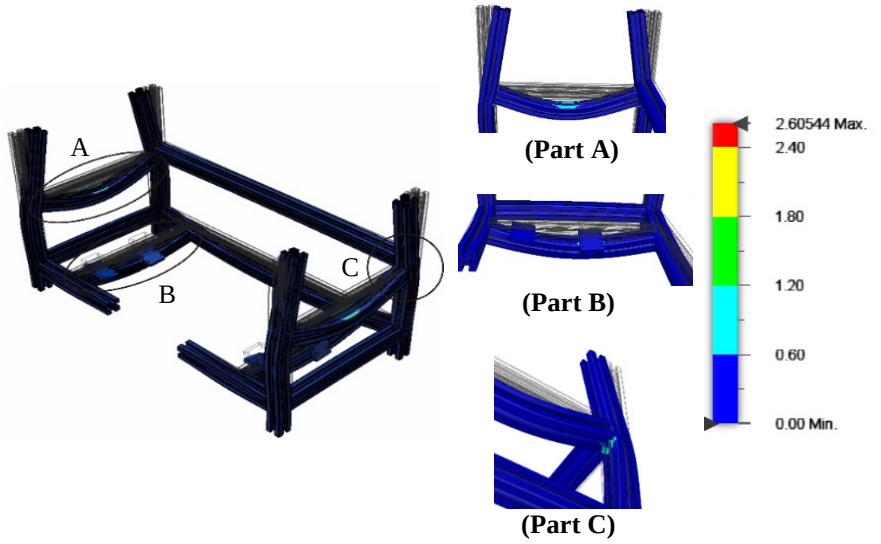

Fig. 17. Frame simulation: stress contour of scenario 2.

The stress analysis of the frame shows that the maximum stress that distributes to the frame has a range from 0-2.605 MPa. It has 0.17 smaller than the first scenario. Results in Fig. 17 indicates that part A has more significant critical stress distribution more than part B due to the downside loads of the second scenario is centred loads of frame mounting. Loads of downside frame are divided into 4 frame mounts, which is different from the first scenario simulation.

7. Conclusions

The auto-checking concept of the hardness machine is proposed to modify the old version of Mitutoyo Hardness Tester HR-522. Improvements of the auto-checking hardness machine is an automatic measurement design which is a large capacity of measurement and faster processing time. Reverse engineering was considered in re-design stage to change the manual hardness tester to the automatic one. The auto checking hardness machine has been appropriated with brake pad hardness checking standard of four-point hardness checking each brake pad. The three axes mechanism of the linear drive is considered in the novel design and replaces the manual devices. The design of the auto checking hardness Machine consists of a frame and linear drives. Results of the governing equation are taken as guidelines to select components of each axis linear drive and linear guides. Results of the frame structure analysis using verified finite element method (FEM) on the proposed auto checking hardness machine based on loads variation involving displacement and maximum stress analyses presented several remarks.

- In the first load scenario, which is a downside distributed load of the frame, produces 1.53×10^{-2} mm in displacement and 2.77 MPa in critical stress.
- The second load scenario, which is a downside centred load of mounting frame results 8.8×10^{-3} mm in displacement and 2.605 MPa in critical stress.

- The overall results of the second load scenario are smaller than the first scenario, which the frame design is more robust against the centred load. Nevertheless, the differences are not significant which implies the frame is well enough to be subject to working loads of the components of auto hardness machine.
- Future research opportunities of the auto checking hardness machine are an analysis of a moving motion and of mechanical materials for the frame as well as break-even point (BEP) analysis as consideration to investment cost.

Acknowledgements

The author's highest appreciation goes to PT. Akebono Brake Astra Indonesia for the research opportunity. The authors also state gratitude for Laboratory of Design and Computational Mechanics, Universitas Sebelas Maret for assistance in design modelling and inspiring discussion of numerical simulation.

Nomenclatures

A	Surface area
d	Penetration diameter on the material (Brinell Hardness)
D	Steel ball diameter
e	Depth of mayor load from the minor load
E	Depth of minor load on the material of zero references
F	Total load
F_0	Minor load
F_1	Mayor load
L	Length

Greek Symbols

σ	Normal stress
τ	Shear stress
ϵ	Strain
δ	Deformation

Abbreviations

BHV	Brinell Hardness Value
HRV	Rockwell Hardness Value
HV	Vickers Hardness Value

References

1. Panda, A.; Sahoo, A.K.; and Rout, A.K. (2017). Machining performance assessment of hardened AISI 52100 steel using multilayer coated carbide insert. *Journal of Engineering Science and Technology*, 12(6), 1488-1505.
2. Mutalib, A.A.; Mussa, M.H.; and Abdulghafoor A.M. (2018). Finite element analysis of composite plate girders with a corrugated web. *Journal of Engineering Science and Technology*, 13(9), 2978-2994.
3. Prabowo, A.R.; Sohn, J.M.; Bae, D.M.; Zakki, A.F.; and Harsritanto, B.I.R. (2018). Investigating crashworthy single and double skin structures against

accidental ship-to-ship interaction. *Curved and Layered Structures*, 5(1), 180-189.

4. Trinade, S.P.; Silva, K.H.S.; Oliveira, D.A.; and Abrão, A.M. (2018). Surface and subsurface alterations induced by hard turning of AISI 52100 bearing steel. *Journal of Engineering Science and Technology*, 13(9), 2765-2778.
5. Prabowo, A.R.; Putranto, T.; and Sohn, J.M. (2019). Simulation of the behavior of a ship hull under grounding: Effect of applied element size on structural crashworthiness. *Journal of Marine Science and Engineering*, 7(8), 270.
6. Fallah, N. (2013). Finite volume method for determining the natural characteristics of structures. *Journal of Engineering Science and Technology*, 8(1), 93-106.
7. Bae, D.M.; Prabowo, A.R.; Cao, B.; Zakki, A.F.; and Haryadi, G.D. (2016). Study on collision between two ships using selected parameters in collision simulation. *Journal of Marine Science and Application*, 15(1), 63-72.
8. Cahn, R.W.; and Haasen, P. (1996). *Physical Metallurgy* (4th ed.). Amsterdam: Elsevier BV.
9. Newage. (2017). *7000 Series Brinell Tester – Operation Manual.* Pennsylvaia: Newage Hardness Testing.
10. Mitutoyo. (2012). *Micro Vickers Hardness Tesing Machines, HM-200 Series.* Kanagawa: Mitutoyo Co.
11. Wilson. (2010). *Rockwell Hardness Tester.* New York.: Wislon Mechanical Instrument Co. Inc.
12. Wang, S.M.; Ye, Z.Z.; Lee, C.Y.; and Wang, C.C. (2016). Design of a micro machine tool with double-toggle mechanisms. *Computational Materials Science*, 117, 549-555.
13. Bohez, E.L.J. (2002). Five-axis milling machine tool kinematic chain design and analysis. *International Journal of Machine Tools and Manufacture*, 42(4), 505-520.
14. Soedarto; Nugroho, H.; Ati, I.M.B.; Febrianty, D.A.; and Widodo, C.E. (2018). *Desain Greenhouse Otomatis Menggunakan Mesin Computer Numerical Control (CNC) Sebagai Lengan Robot Terintegrasi Software BLYNK pada Smartphone Android Guna Meningkatkan Produktivitas Pertanian Holtikultura*. Hak Kekayaan Intelektual, Kementrian Hukum dan HAM. 2018/S/00883 (in Indonesian).
15. LPPM Universitas Riau, Laka, O.; Sudariyanto; Dapa, A.P.; and Syafri. (2019). *Inovasi Pemanfaatan Limbah Elektronik Menjadi Prototipe Mesin CNC 3 Axis Sebagai Media Edukasi.* Hak Kekayaan Intelektual, Kementrian Hukum dan HAM. 2019/S/00499 (in Indonesian).
16. Wredenberg, F.; and Larsson, P. (2009). Scratch testing of metals and polymer: Experiments and numerics. *Wear*, 266(1-2), 76-83.
17. ASTM International, *Standard Test Methods ASTM-E18 for Rockwell Hardness of Metallic Materials*. Pennsylvania: ASTM International.
18. ASTM International, *Standard Test Method ASTM-E10 for Brinell Hardness of Metallic Material.* Pennsylvania: ASTM International.
19. ASTM International, *Standard Test Method ASTM-E384 for Micro Indentation Hardness of Materials*, Pennsylvania: ASTM International.

20. Guo, B.; Zhang, L.; Cao, L.; Zhang, T.; Jiang, F.; and Yan, L. (2018). The correction of temperature-dependent Vickers hardness of cemented carbide base on the developed high-temperature hardness tester. *Journal of Materials Proceding Technology*, 255, 426-433.
21. Allen, R. (2006). A guide to rebound hardness and scleroscope test. Retrieved November 6, 2019, from http://ra1.articlealley.com/a-guide-to-rebound-hardness-and-scleroscope-test-111192.html.
22. Batan, I.M.L. (2012). *Desain Produk.* (1st ed.). Surabaya: Guna Widya (in Indonesian).
23. Husain, Z.; Jan, H. (2019). Establishing simulation model for optimizing efficiency of CNC machine using reliability-centered maintenance approach. *International Journal of Modeling, Simulation, and Scientific Computing*, 10(6), 1950034.
24. Wang, W.; and Zhang, Y. (2017). Dynamic Reliability Analysis of Linear Guides in Positioning Precision. *Mechanism and Machine Theory*, 116, 451-464.
25. Misumi (2019). *Mechanical Automation Components* (10th ed.). Schaumburg: Misumi USA.
26. Beer, F.P. (2013). *Vector Mechanics for Engineers Statics and Dynamics* (11th ed.). New York: McGraw-Hill.
27. Beer, F.P.; Johnston, E.R.; Dewolf, J.T.; and Mazurek, D.F. (2012). *Mechanics of Material* (6th ed.). New York: McGraw-Hill.
28. Baptista, R.J.S.; Pragana, J.P.M.; Bragança, I.M.F.; Silva, C.M.A.; Alves, L.M.; and Martins, P.A.F. (2020). Joining Aluminum Profiles to Composite Sheets by Additive Manufacturing and Forming. *Journal of Materials Processing Tech*nology, 279, 116587.
29. Hong, C.C.; Chang, C.L.; and Lin, C.Y. (2016). Static structural analysis of great five-axis turning-milling complex CNC machine. *Engineering Science and Technology, an International Journal*, 19(4), 1971-1984.
30. Hidayat, T.; Nazaruddin, N.; and Syafri S. (2017). Perancangan dan Analisis Statik Chassis Kendaraan Shell Eco Marathon Tipe Urban Concept. *Jurnal Online Mahasiswa Fakultas Teknik Universitas Riau*, (4)2, 1-6 (in Indonesian).
31. Francoisa, P.; Palit, A.; Gerbino, S.; and Ceglarek, D. (2019). A novel hybrid shell element formulation (QUAD+ and TRIA+): A benchmarking and comparative study. *Finite Elements in Analysis and Design*, 166, 103319.
32. Prabowo, A.R.; Cahyono, S.I.; and Sohn, J.M.; (2019). Crashworthiness assessment of thin-walled double bottom tanker: A variety of ship grounding incidents. *Theoretical and Applied Mechanics Letters*, 9(5), 320-327.
33. Muttaqie, T.; Thang D.Q.; Prabowo, A.R.; Cho, S.R.; and Sohn, J.M. Numerical studies of the failure modes of ring-stiffened cylinders under hydrostatic pressure. *Structural Engineering and Mechanics*, 70(4), 431-443.
34. Rino, W.S.; Andias, A.; and Ilma, M. (2015). The design of batik stamp tool scraping working table using ergonomics principles. *Procedia Manufacturing*, 4, 543-551.
35. Du, Z.; Duan, L.; Cheng, A.; Xu, Z.; and Zhang, G. (2019). Theoretical prediction and crashworthiness optimization of thin-walled structures with

single-box multi-cell section under three-point bending loading. *International Journal of Mechanical Sciences*, 157, 703-714.

36. Tanojo, E.; Pudjisuryadi, P.; and Candra, B.P.; and William, W. (2015). Design capacity tables for structural steel based on SNI 03-1729-2002: Built up sections. *Procedia Engineering*, 125, 1142-1148.
37. Onyenanu, I.U.; Swift, O.N.K.; and Atanmo, P.N. (2015). Design and analysis of a tubular space frame chassis for FSAE application. *Journal of Emerging Technologies and Innovative Research*, 2(10), 134-140.
38. Ellingwood, B.; and Galambos, T.V. (1982) Probability-based criteria for structural design. *Structural Safety*, 1(1), 15-26.